Control of a DFIG based wind turbine using modified Conditional Servo-compensator

Vancuong Nguyen, Mariana Netto, Gilney Damm

▶ **To cite this version:**

Vancuong Nguyen, Mariana Netto, Gilney Damm. Control of a DFIG based wind turbine using modified Conditional Servo-compensator. 22nd World Congress of the International Federation of Automatic Control (IFAC 2023), IFAC, Jul 2023, Yokohama, Japan. 10.1016/j.ifacol.2023.10.1167 . hal-04215806

HAL Id: hal-04215806
https://hal.science/hal-04215806

Submitted on 22 Sep 2023

HAL is a multi-disciplinary open access archive for the deposit and dissemination of scientific research documents, whether they are published or not. The documents may come from teaching and research institutions in France or abroad, or from public or private research centers.

L'archive ouverte pluridisciplinaire **HAL**, est destinée au dépôt et à la diffusion de documents scientifiques de niveau recherche, publiés ou non, émanant des établissements d'enseignement et de recherche français ou étrangers, des laboratoires publics ou privés.

Control of a DFIG based wind turbine using modified Conditional Servo-compensator

Van Cuong Nguyen * **Mariana Netto** ** **Gilney Damm** ***

* *L2S - Paris-Saclay University, Gif-sur-Yvette, France (e-mail: vancuong.nguyen@centralesupelec.fr)*
** *COSYS-PICS-L, Univ. Gustave Eiffel, IFSTTAR, F-78000 Versailles, France (e-mail: mariana.netto@univ-eiffel.fr)*
*** *COSYS-IMSE, Univ. Gustave Eiffel, IFSTTAR, F-77447 Marne-la-Vallée, France, (e-mail: gilney.damm@univ-eiffel.fr)*

Abstract: This paper presents the control of a wind turbine composed by a doubly fed induction generator (DFIG), which provides power to the main grid through a feeder. The control algorithm is designed following the modified Conditional Servo-Compensator (mCS) theory. This control technique was recently developed to a broad class of nonlinear systems, and this paper brings the first result applied to wind turbines. The mCS theory has several advantages compared to others, as it is a robust nonlinear control scheme. First, it provides rigorous stability analysis, that allows explicit definition of performance and operating conditions. Secondly, it is a robust controller, and only needs lump values and bounds for parameters and dynamics. Finally it is very simple and easy to implement, and does not need heavy computer burden, it is only based on standard local measurements, and represents a promising solution for real applications. The theoretical results are verified by simulations using detailed Simpower models. These simulations show very good results facing a Low Voltage Ride Through scenario, which is one of the most severe tests used for practical applications. The proposed scheme could easily be adapted to the control of other applications based on power converters, as the control of the interconnection of a full wind farm to the main grid, or the control of a terminal in a DC grid.

Keywords: Control of renewable energy resources; Control of power systems; Nonlinear control; Application of power electronics; Control system design

1. INTRODUCTION

Doubly fed induction generator (DFIG) wind turbines are one of the standards in the case of medium to large turbines (Muller et al. [2002]). With the continuous increase of wind generation, new grid codes in many countries require wind turbines to remain connected during grid faults, for example severe voltage drops (Low Voltage Ride Through), and to contribute to system stability after fault clearance. Such faults represents a major challenge for wind turbine control, and are capital for the future connection of large DFIG wind turbines to the main Alternative Current (AC) grid. In fact, there is great concern about grid stability since the large penetration of renewable energy sources and power electronic devices (ENTSO-E [2022]), in particular since the 2019 UK black-out, largely caused by wind turbines disconnection (OFGEN [2019]).

Several research groups have been addressing this issue from different points of view. Classic results have suggested improving generator's terminal voltage during a grid fault using shunt reactive power compensation (Anaya-Lara and Jenkins [2005]), or the use of a crowbar (Pannell et al. [2005]). More recent results have rather addressed the improvement using better control strategy (De Souza et al. [2022], Din et al. [2021]), which is also the goal of the present work.

There exist numerous control strategies for DFIG wind farms. Most of them are composed of PID, and are based on a time-scale separation, considering that currents have much faster dynamics than the DC Voltage (Chen et al. [2020]). Therefore a control structure with an inner current control loop and an outer DC voltage control loop is commonly proposed, and is frequently called vector control, but indeed is composed of PID controllers in either loops (Muller et al. [2002], Miller et al. [2003], Pena et al. [1996] and Hansen and Michalke [2007]). However, tuning coupled PID controllers can be quite challenging; it is only possible to ensure stability in a very small operation region; in general it can not analytically be established an operation region; it is not provided rules on how to tune these controllers.

In our work, the modified Conditional Servo-compensator (mCS) strategy is proposed for DFIG wind farm. The present controller is developed in (Damm and Nguyen [2012], Nguyen [2013]) for Multi-Input Multi-Output uncertain nonlinear systems based on (Khalil [2000], Khalil [2001]). The Conditional Servo-Compensator (CS) theory says that if a MIMO uncertain nonlinear system satisfies

some basic conditions, then the application of this control strategy gives a globally exponential stability of the closed-loop system. The controller is designed such as to behave as a dynamic linear controller inside an arbitrary region, and as a robust nonlinear one in the remaining domain. For DFIG wind turbines which are uncertain and perturbed by external signals, the modified Conditional Servo-Compensator can guarantee the global exponential stability with a rigorous mathematical analysis.

The structure of the paper is as follows: Section 2 describes a DFIG wind turbine and its mathematical model. In Section 3 the mCS Control is developed and applied to control the grid side and the rotor side of the back to back power converter. The performance of the proposed controller for the wind farm in the case of low voltage ride-through is illustrated by simulation results in Section 4. These simulations are performed using SimPowerSystems toolbox. The paper ends by conclusions in Section 5.

2. DYNAMIC MODEL OF DFIG

2.1 Grid side converter

The schematic diagram of a double fed induction machine (DFIM) based wind turbine is shown in Fig. 1. It is composed of an induction machine with its stator directly connected to the grid, and its rotor windings connected to a back to back Voltage Source Converter (VSC) which is then connected to the main grid. The objective of the grid side converter (right side DC/AC stage of the full converter) is to keep the DC voltage constant regardless of the rotor power, and to control the reactive power delivered to the main AC grid. We introduce an averaged state space model of the grid side converter established in a dq reference frame (Padiyar and Prabhu [2004]), where ω_b is the base constant for the per unit transformation for the grid frequency ($50Hz$ or $60Hz$), $\bar{\omega}$ the per unit value for grid frequency, $v_{l,dq}$ are the voltages of the grid, R_{pu} and L_{pu} represent series connected phase reactors, $v_{c,dq}$ are the voltages at the grid side of the converter, $i_{l,dq}$ are the currents through the phase reactors, u_c is the DC voltage, C is the DC capacitor and i_c is the DC bus current. All variables are calculated in per unit system (Abad et al. [2011]).

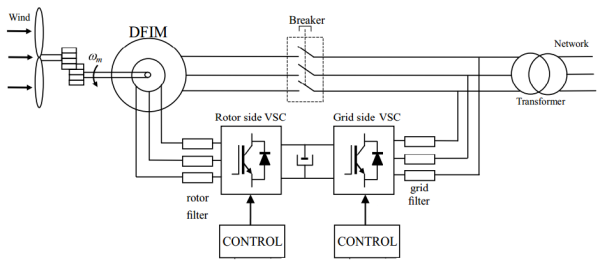

Fig. 1. DFIM wind turbine schematic

The average model in pu for the AC side of the converter is written as:

$$\begin{aligned}\frac{di_{ld}}{dt} &= -\omega_b \frac{R_{pu}}{L_{pu}} i_{ld} + \bar{\omega}\omega_b i_{lq} - \frac{\omega_b}{L_{pu}}(v_{cd} - v_{ld}) \\ \frac{di_{lq}}{dt} &= -\omega_b \frac{R_{pu}}{L_{pu}} i_{lq} - \bar{\omega}\omega_b i_{ld} - \frac{\omega_b}{L_{pu}}(v_{cq} - v_{lq})\end{aligned} \tag{1}$$

The instantaneous active power P and the reactive power Q on the AC side can be written as:

$$P = v_{ld} i_{ld} + v_{lq} i_{lq}; \quad Q = v_{lq} i_{ld} - v_{ld} i_{lq} \tag{2}$$

where we have taken the standard consideration that the d axis of the dq reference frame is chosen such that it is fixed to the AC grid voltage. For this reason, in normal operation, $v_{ld} = 1$ and $v_{lq} = 0$, and it can be used the control strategy of steering i_{ld} to drive the DC voltage and i_{lq} to drive the reactive power, as it will be seen in the following.

Losses on the converter are usually small compared to the active power, and in most cases we can neglect these converter's losses. Taking into account the power balance on the AC and DC sides, the DC voltage (considered always positive) can be written as:

$$C\frac{du_c^2}{dt} = (v_{ld} i_{ld} + v_{lq} i_{lq}) - i_c u_c \tag{3}$$

2.2 Rotor side converter

Since the stator is connected to the grid, and the influence of the stator resistance is small, the stator flux can be considered as constant. Under stator flux orientation, the relationship between the voltages, currents and fluxes may be written as (Abad et al. [2011]):

$$T_e = -\frac{L_m}{L_s} \psi_s i_{rq} \tag{4}$$

representing the rotor torque, such that the currents are:

$$\begin{aligned}\frac{di_{rd}}{dt} &= -\omega_b \frac{R_{ru}}{\varsigma L_{ru}} i_{ld} + \bar{\omega}_s \omega_b i_{lq} - \frac{\omega_b}{\varsigma L_{ru}} v_{rd} \\ \frac{di_{rq}}{dt} &= -\omega_b \frac{R_{ru}}{\varsigma L_{ru}} i_{rq} - \bar{\omega}_s \omega_b i_{ld} - \bar{\omega}_s \psi_s + \frac{\omega_b}{\varsigma L_{ru}} v_{rq}\end{aligned} \tag{5}$$

where ς is the leakage factor. The stator flux angle is calculated from:

$$\begin{cases} \psi_{\alpha s} = \int (v_{\alpha s} - R_{pu} i_{\alpha s}) dt \\ \psi_{\beta s} = \int (v_{\beta s} - R_{pu} i_{\beta s}) dt \end{cases} \Rightarrow \theta_s = \tan^{-1}(\psi_{\beta s}/\psi_{\alpha s}) \tag{6}$$

where $i_{r,dq}$ is the rotor current, $v_{r,dq}$ the rotor voltage, ψ_s the stator flux and $\bar{\omega}_s$ the slip frequency in the stator flux orientation. R_{ru} and L_{pu} are the resistance and inductance of the rotor.

3. CONDITIONAL SERVO-COMPENSATOR CONTROL

The MIMO Conditional Servo-compensator controller design for the output regulation of a class of minimum-phase nonlinear systems in case of asymptotically constant references is studied in (Mahmoud and Khalil [1997]), (Khalil [2000]) and in (Damm and Nguyen [2011]). These papers concern a servo-compensator performing as a nonlinear robust controller outside a boundary layer, and performing as a dynamic linear controller inside it. First results have studied the SISO case and were extended in (Seshagiri

and Khalil [2005]) and in (Memona and Khalil [2010]) for linear MIMO systems under some additional assumptions. Finally these results were extended for a class of MIMO nonlinear systems in (Damm and Nguyen [2012]). The present case however needs some new developments on those previous results in order to address the present case.

3.1 Conditional Servo-Compensator control

Consider the system:

$$\dot{e} = f(e) + g(e)u \tag{7}$$

where $e(t) \in \mathbb{R}^n$ is an error vector, $u \in \mathbb{R}^n$ is the control input and $f(e) \in \mathbb{R}^n$, $g(e) \in \mathbb{R}^{n\times n}$ are continuous functions. Let us define an error-measurement surface as:

$$\varphi = K_0\sigma + e \tag{8}$$

where $\sigma \in \mathbb{R}^n$ is the output of the conditional servo-compensator:

$$\dot{\sigma} = -K_0\sigma + \mu \text{sat}(\varphi/\mu) \tag{9}$$

in which μ is the boundary layer, K_0 is a positive definite matrix.

Assumption 3.1. $f(e)$ is bounded by a function $\gamma_f(e)$ (where γ_f is a class $\mathcal{K}$ function) and a positive constant δ_0:

$$\|f(e)\| \leq \gamma_f(e) + \delta_0 \tag{10}$$

for $e \in \mathbb{R}^n$, and as a consequence:

$$\|f(e=0)\| = \|f(0)\| \leq \delta_0.$$

And in the neighborhood region of the equilibrium point $e = 0$, f and γ_f are Lipschitz:

$$\|f(e)\| \leq c_f\|e\|; \;\; \|\gamma_f(e)\| \leq c_{\gamma_f}\|e\| \tag{11}$$

Assumption 3.2. $g(e)$ is continuous and invertible for all $e \in \mathbb{R}^n$.

Theorem *3.1.* Consider the nonlinear system in (7) where the function $f(e)$ satisfies Assumption 3.1, and the function $g(e)$ satisfies Assumption 3.2, with the error surface defined in (8). Then control law:

$$\begin{cases} u = -\Pi(e)\text{sat}(\varphi/\mu) \\ \Pi(e) = [g(e)]^{-1}(\Pi_0 + \mu K_0 + (\gamma(e) + \delta_0)I_n) \end{cases} \tag{12}$$

where Π_0 is a positive definite matrix, $I_n \in \mathbb{R}^{nxn}$ the identity matrix and γ is a function yet to be defined, rends the closed-loop system exponentially stabilized to its origin.

Proof: Without loss of generality we will first consider the case where the error's initial conditions, represented by the integral error measurement surface φ, are large.

Considering the region $\|\varphi\| \geq \mu$, $sat(\varphi/\mu) = \varphi/\|\varphi\|$.

The derivative of the integral error measurement surface may be expressed as

$$\dot{\varphi} = K_0\dot{\sigma} + \dot{e} \tag{13}$$

which, in view of (9) and (7), is equivalent to

$$\dot{\varphi} = -K_0\varphi + \mu K_0 sat(\varphi/\mu) + K_0 e + f(e) + g(e)u \tag{14}$$

Furthermore, define an intermediate function $\delta : \mathbb{R}^n \to \mathbb{R}^n$

$$\delta(e) = K_0 e + f(e) \tag{15}$$

then using Assumption (3.1), δ satisfies

$$\|\delta(e)\| \leq \|K_0 e\| + \gamma_f(e) + \delta_0 = \gamma(e) + \delta_0 \tag{16}$$

where the function γ aforementioned in (12) is,

$$\gamma(e) = \|K_0 e\| + \gamma_f(e) \tag{17}$$

Equation (14) becomes

$$\dot{\varphi} = -K_0\varphi + \mu K_0 sat(\varphi/\mu) + \delta(e) + g(e)u \tag{18}$$

The product $\varphi^T\dot{\varphi}$ may be computed using Assumption 3.1, the control law (12) and the saturation function to obtain:

$$\varphi^T\dot{\varphi} \leq -\lambda_{min}(\Pi_0)\|\varphi\| \Rightarrow \frac{d(\|\varphi\|)}{dt} \leq -\lambda_{min}(\Pi_0)$$
$$\Rightarrow \|\varphi(t)\| \leq \|\varphi(0)\| - \lambda_{min}(\Pi_0)t.$$

Then, the trajectories on the integral error measurement surface φ reach the set:

$$\mathcal{O}_\varphi = \{\varphi \in R^n \mid \|\varphi\| \leq \mu\} \tag{19}$$

in finite time.

Considering the region $\|\varphi\| \leq \mu$, $sat(\varphi/\mu) = \varphi/\mu$ Consider again (8), (9), (18) and the control law (12), which inside the boundary layer may be rewritten as:

$$\begin{cases} \dot{\sigma} = -K_0\sigma + \varphi \\ \dot{\varphi} = \delta(e) - g(e)\Pi(e)\varphi/\mu \\ e = \varphi - K_0\sigma \end{cases} \tag{20}$$

It can be shown that this system has the equilibrium point:

$$\begin{cases} \varphi = \bar{\varphi}, \quad \sigma = \bar{\sigma} \\ \bar{\varphi} = K_0\bar{\sigma} = [\Pi_0 + \mu K_0 + \delta_0 I_n]^{-1} f(0) \end{cases} \tag{21}$$

The system (20) may then be rewritten with respect to $\bar{\varphi}$ and $\bar{\sigma}$:

$$\begin{cases} \dot{\tilde{\sigma}} = -K_0\tilde{\sigma} + \tilde{\varphi} \\ \dot{\tilde{\varphi}} = \delta(e) - \Pi(e)g(e)\tilde{\varphi}/\mu - \Pi(e)g(e)\bar{\varphi}/\mu \\ e = \tilde{\varphi} - K_0\tilde{\sigma} \end{cases} \tag{22}$$

where $\tilde{\sigma} = \sigma - \bar{\sigma}$, $\tilde{\varphi} = \varphi - \bar{\varphi}$.

We would like to demonstrate that every trajectory of (22) starting inside the boundary layer, approaches the equilibrium point $(\tilde{\sigma}, \tilde{\varphi}) = (0, 0)$ as time tends to infinity. Towards that end, we take:

$$W = \frac{1}{2}\tilde{\sigma}^T K_0\tilde{\sigma} + \frac{1}{2}\tilde{\varphi}^T\tilde{\varphi} \tag{23}$$

as a Lyapunov candidate.

Since $\delta(e)$ in (15) can be rewritten as:

$$\delta(e) = K_0\tilde{\varphi} - K_0^2\tilde{\sigma} + f(e). \tag{24}$$

So the derivative of the Lyapunov candidate yields:

$$\begin{aligned} \dot{W} = &-\tilde{\sigma}^T K_0^2\tilde{\sigma} - \tilde{\sigma}^T K_0(K_0 - I_n)\tilde{\varphi} + \tilde{\varphi}^T K_0\tilde{\varphi} \\ &-\tilde{\varphi}^T g(e)\Pi(e)\bar{\varphi}/\mu) + \tilde{\varphi}^T(f(e) - g(e)\Pi(e)\bar{\varphi}/\mu) \end{aligned} \tag{25}$$

After some intermediate steps, omitted here for the sake of brevity, the derivative of W can be developed as (where m_1, l_σ and l_s are positive constants):

$$\dot{W}\leq -(\frac{1}{2}-\frac{1}{2m_1}-l_\sigma)\tilde{\sigma}^T K_0^2\tilde{\sigma} \\ -\tilde{\varphi}^T(g(e)\Pi(e)/\mu-(K_0+\frac{m_1}{2}(K_0-I_n)^2+l_sI_n))\tilde{\varphi}$$

In order to obtain a negative derivative of the Lyapunov candidate $\dot{W}$ for all $\tilde{\varphi}$ and $\tilde{\sigma}$, it is necessary to impose design conditions, that are simplified if one considers the fact that l_s and l_σ are significantly small when the attractive region is small, leading to:

$$\begin{cases} m_1 & > & 1 \\ (\Pi_0+\delta_0 I_n)/\mu & > & \frac{m_1}{2}(K_0-I_n)^2 \end{cases} \tag{26}$$

These conditions are satisfied by taking m_1 and $\|\Pi_0\|$ large enough with respect to control dynamics, or conversely by taking μ small enough. In this way, $W(t)$ satisfies $W(t)>0$ and $\dot{W}<-w_0W$ (where w_0 is a positive constant) for all $\sigma\neq\bar{\sigma}$ and $\varphi\neq\bar{\varphi}$. Then $W(t)$ exponentially converges to zero when time tends to infinite. As a consequence, the output error $e(t)=\tilde{\varphi}-K_0\tilde{\sigma}$, exponentially converges to 0. We assure the exponential stability of the equilibrium point $(\bar{\sigma},\bar{\varphi},0)$ of system (22) in the region of $\|\varphi\|\leq\mu$. As a consequence, system (7) is exponentially stable.

Remark 1. This result improves those in (Damm and Nguyen [2012]) in the fact that in those results function $g(e)$ was required to be known (even if uncertain), while in the present result, it is only required to be continuous and non-singular.

3.2 Control of grid side converter

Current loop control Taking the per-unit error dynamics of currents of the VSC terminal in (1) according to their constant reference signals $i_{ld,r}$ and $i_{lq,r}$:

$$\frac{d\tilde{i}_{ldq}}{dt}=A\tilde{i}_{ldq}+Ai_{ldq,r}+B\tilde{v}_{cdq} \tag{27}$$

where $i_{ldq}=[i_{ld},i_{lq}]$, $i_{ldq,r}=[i_{ld,r},i_{lq,r}]$, $\tilde{i}_{ldq}=i_{ldq}-i_{ldq,r}$, $\tilde{v}_{cdq}=v_{cdq}-v_{ldq}$ and:

$$A=\begin{bmatrix} -\omega_b\frac{R_{pu}}{L_{pu}} & \bar{\omega}\omega_b \\ -\bar{\omega}\omega_b & -\omega_b\frac{R_{pu}}{L_{pu}} \end{bmatrix};\quad B=\begin{bmatrix} -\frac{\omega_b}{L_{pu}} & 0 \\ 0 & -\frac{\omega_b}{L_{pu}} \end{bmatrix}.$$

Equation (1) can be rewritten as:

$$\frac{d\tilde{i}_{ldq}}{dt}=\zeta_f(\tilde{i}_{ldq})+\zeta_g(\tilde{i}_{ldq})\tilde{v}_{cdq} \tag{28}$$

Function ζ_f is bounded by a scalar function γ_f and a positive constant δ_0

$$\|\zeta_f(\tilde{i}_{ldq})\|\leq\gamma_f(\tilde{i}_{ldq})+\delta_0; \tag{29}$$

ζ_f then satisfies Assumption 3.1.

Matrix ζ_g is invertible, then it satisfies Assumption 3.2.

Since system (28) has ζ_f and ζ_g satisfying Assumptions 3.1 and 3.2, application of the Conditional Servo-compensator control to (28) can be expressed as:

$$\begin{cases} \tilde{v}_{cdq}=-\Pi(\tilde{i}_{ldq})\text{sat}(\varphi/\mu) \\ \dot{\Pi} \quad =-\frac{L_{pu}}{\omega_b}(\Pi_0+\mu K_0+(\gamma(\tilde{i}_{ldq})+\delta_0)I_2) \end{cases} \tag{30}$$

where $[\zeta_g]^{-1}=-\frac{L_{pu}}{\omega_b}I_2$ and $\delta_0=\sqrt{(\bar{\omega}\omega_b)^2+(\omega_b\frac{R_{pu}}{L_{pu}})^2}$.

Let us consider conditions for the controller's parameters Π_0, K_0 and μ stated in (26). We take $m_1=3/2$, and then (26) becomes:

$$(\Pi_0+\sqrt{(\bar{\omega}\omega_b)^2+(\omega_b\frac{R_{pu}}{L_{pu}})^2}I_2)/\mu>\frac{3}{4}(K_0-I_n)^2 \tag{31}$$

Taking into account the neglected effect of l_s on the inequality (26), Π_0 must be large enough and μ small enough. We then take $\mu=0.5$ for the boundary layer and $\Pi_0=2\delta_0I_2$.

Value K_0 is tuned small satisfying

$$\begin{cases} \mu K_0 << \mu\omega_bI_2<0.5\sqrt{(\bar{\omega}\omega_b)^2+(\omega_b\frac{R_{pu}}{L_{pu}})^2}=0.5\delta_0 \\ \|K_0\|<<\omega_b<\sqrt{(\bar{\omega}\omega_b)^2+(\omega_b\frac{R_{pu}}{L_{pu}})^2} \end{cases} \tag{32}$$

Terms μK_0 and $\|K_0\|$ can be neglected, and

$$\Pi(\tilde{i}_{ldq})=-\sqrt{(L_{pu})^2+(R_{pu})^2}(\|\tilde{i}_{ldq}\|+3)I_2 \tag{33}$$

DC voltage loop Considering again the per-unit dynamics of the DC voltage side in (3) according to its constant reference signal $u_{c,r}$,

$$C_{pu}\frac{de_u}{dt}=-i_c(u_c-u_{c,r})-i_cu_{c,r}+v_{ld}(i_{ld}+\frac{v_{lq}}{v_{ld}}i_{lq}) \tag{34}$$

where $e_u=u_c^2-u_{c,r}^2$.

Let us define $i_u=(i_{ld}+\frac{v_{lq}}{v_{ld}}i_{lq})$ as the control input, previous equation can be stated as,

$$\frac{de_u}{dt}=f_u(e_u)+g_u(e_u)i_u \tag{35}$$

where

$$f_u(e_u)=-(i_c(u_c-u_{c,r})+i_cu_{c,r})/C_{pu} \tag{36}$$

$$g_u(e_u)=v_{ld}/C_{pu}. \tag{37}$$

One can show that f_u satisfies Assumption 3.1, and function g_u is invertible and satisfies Assumption 3.2, so, application of mCS control to (35) yields:

$$\begin{cases} i_u \quad =-\Pi(e_u)\text{sat}(\varphi/\mu) \\ \Pi(e_u)=(\frac{1}{u_{c,r}}|e_u|+9/8|u_{c,r}|)/v_{ld} \end{cases} \tag{38}$$

3.3 Control of rotor side

Now considering the per-unit dynamics of currents of the rotor side in (5) according to their constant reference signals $i_{rd,r}$ and $i_{rq,r}$:

$$\frac{d\tilde{i}_{rdq}}{dt}=A\tilde{i}_{rdq}+Ai_{rdq,r}+Bv_{rdq} \tag{39}$$

where $i_{rdq} = [i_{rd}, i_{rq}]$, $i_{rdq,r} = [i_{rd,r}, i_{rq,r}]$, $\tilde{i}_{rdq} = i_{rdq} - i_{rdq,r}$ and :

$$A = \begin{bmatrix} -\omega_b \frac{R_{ru}}{\varsigma L_{ru}} & \bar{\omega}_s \omega_b \\ -\bar{\omega}_s \omega_b & -\omega_b \frac{R_{ru}}{\varsigma L_{ru}} \end{bmatrix}; B = \begin{bmatrix} -\frac{\omega_b}{\varsigma L_{ru}} & 0 \\ 0 & -\frac{\omega_b}{\varsigma L_{ru}} \end{bmatrix}.$$

After a similar computation as in section 3.2.1, the mCS controller for the rotor side can be stated as:

$$\Pi(\tilde{i}_{ldq}) = -\frac{L_{pu}}{\omega_b}(\mu K_0 + 3\delta_0 I_2 + \|\tilde{i}_{ldq}\|(\|K_0\| + \sqrt{(\bar{\omega}\omega_b)^2 + (\omega_b \frac{R_{pu}}{L_{pu}})^2) I_2}) \quad (40)$$

4. SIMULATION RESULTS

In this Section, the proposed control strategy designed in previous sections is applied to a 1.5 MW wind farm connected to a 25KV/60Hz distribution system that exports power to a 120kV grid through a 30km, 25kV feeder (see Fig. 2). The simulation is illustrated using the detailed Matlab/Simulink SimScape Electrical Toolbox. In this simulation, the wind speed is maintained constant at 15m/s. A PID controls the rotor torque in order to maintain the turbine speed as 1.2pu. The reactive power produced by the wind turbine is regulated at 0Mvar for the grid side. The simulation illustrates the performance of the proposed controllers through voltage drop at the grid from 1.0pu to 0.5pu programmed at t=0.23s and voltage step up to 1.0pu after 0.1s. Fig. 3 shows that the grid voltage from the steady state drops to 0.4pu during the interval 0.23s to 0.33s.

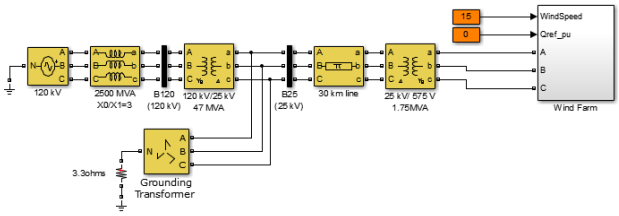

Fig. 2. DFIG wind turbine connected to a distribution system

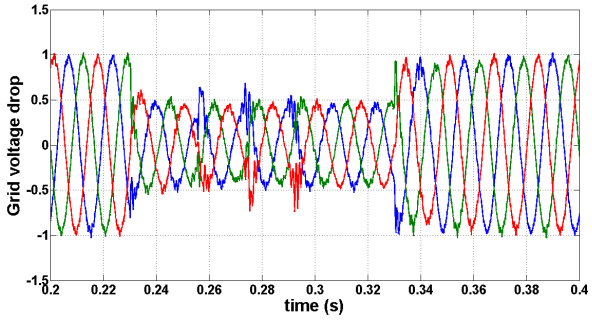

Fig. 3. Grid voltage drop from 1.0pu to 0.4pu

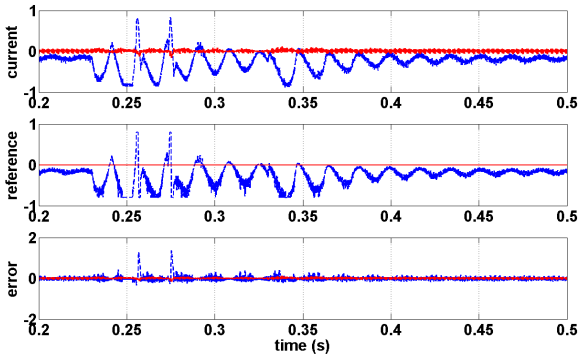

Fig. 4. $i_{l,dq}$ current in dq frame

Fig. 4 illustrates the simulation results of the grid side's current when applied the proposed controllers for the current loop. i_{lq} current is set to zero to give a zero reactive power. The i_{ld} current reference from the DC voltage loop is followed by its actual value. The zero current error shows the regulation performance of the current loop control by mCS.

Fig. 5 shows the DC voltage at the capacitor during grid voltage drop. The DC voltage satisfies the grid code which requires the DC voltage to stay in $0.9pu$ to $1.1pu$ during the voltage drop. A small oscillation on the DC voltage is explained from the change of rotor speed which results in oscillation of rotor current.

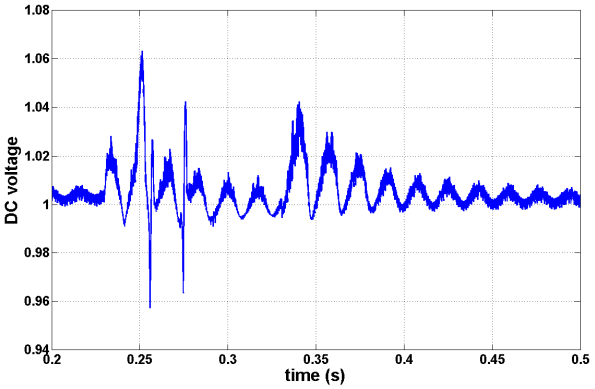

Fig. 5. DC voltage of the capacitor

The rotor current loop control aims to keep active and reactive power at the same value during the grid voltage drop. Figs. 6 and 7 shows the currents and the active power. Fig. 6 illustrates how the mCS controller allows the rotor currents to follow their references, and the active power to converge to 1.0pu after the grid voltage drop.

5. CONCLUSION

This paper has presented the development of a mCS Controller for a DFIG wind turbine. The work has demonstrated that the DFIG wind turbine satisfies the sufficient conditions of this theory, and as a consequence can be controlled by mCS controllers for current and DC voltage loops in the grid side and for the rotor currents in the rotor side. The simulation results have shown that the

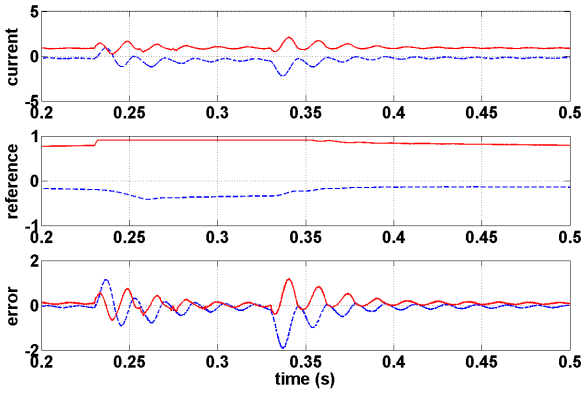

Fig. 6. $i_{r,dq}$ current in dq frame

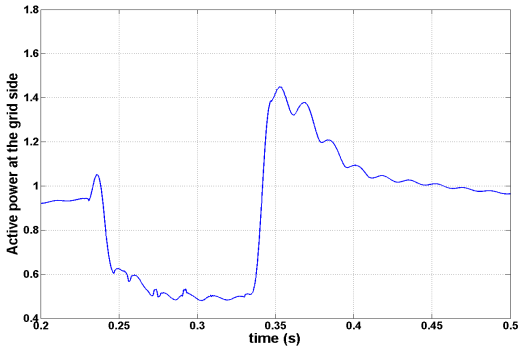

Fig. 7. Active power of the grid side

controller is robust and performs well for the severe test of low voltage ride through scenario. An important advantage of the mCS controller is the easiness for its application and for tuning its parameters. In future works it will be investigated its application for other topologies of wind turbines and other electrical systems.

REFERENCES

Gonzalo Abad, Jesus Lopez, Miguel Rodríguez, Luis Marroyo, and Grzegorz Iwanski. *Doubly fed induction machine: modeling and control for wind energy generation*, volume 85. John Wiley & Sons, 2011.

O Anaya-Lara and N Jenkins. Fault current contribution of dfig wind turbines. *IEE Conf. Reliability of Transmission and Distribution Networks, London*, 2005.

Yijing Chen, Miguel Jiménez Carrizosa, Gilney Damm, Françoise Lamnabhi-Lagarrigue, Ming Li, and Yan Li. Control induced time-scale separation for multi-terminal high voltage direct current systems using droop control. *IEEE Transactions on Control Systems Technology*, 28 (3):967–983, May 2020.

Gilney Damm and Van Cuong Nguyen. Mimo conditional integrator control for a class of nonlinear systems. In *In proceedings of System Theory, Control, and Computing (ICSTCC), 2011 15th International Conference, Sinaia, Romania*, October 14-16 2011.

Gilney Damm and Van Cuong Nguyen. Mimo conditional servo-compensator control for a class of nonlinear systems. *In Proceedings of the 51th Conference on Decision and Control, Maui - Hawaii, USA.*, December 10-13 2012.

Victor Ramon F. B. De Souza, Luciano S. Barros, Flavio B. Costa, and Guilherme P. Da Silva Junior. Doubly fed induction generator low voltage ride through improvement through modular multilevel converter. *IEEE Access*, 10:57914–57929, 2022.

Zakiud Din, Jianzhong Zhang, Zheng Xu, Yaqian Zhang, and Jin Zhao. Low voltage and high voltage ride-through technologies for doubly fed induction generator system: Comprehensive review and future trends. *IET Renewable Power Generation*, 15(3):614–630, 2021. doi: https://doi.org/10.1049/rpg2.12047.

European Network Transmission System Operators ENTSO-E. Stability management in power electronics dominated systems: A prerequisite to the success of the energy transition. *ENTSO-E Position Paper*, 1:16, 2022.

Anca D Hansen and Gabriele Michalke. Fault ride-through capability of dfig wind turbines. *Renewable energy*, 32 (9):1594–1610, 2007.

Hassan K. Khalil. On the design of robust servomechanisms for minimum phase nonlinear systems. *Robust Nonlinear Control 2000, John Wiley & Sons*, 10:339–361, 2000.

Hassan K. Khalil. *Nonlinear Systems*. Prentice Hall, 2001.

Nazmi A. Mahmoud and Hassan K. Khalil. Robust control for a nonlinear servomechanism problem. *International Journal of Control*, 66:779–802, April 1 1997.

Attaullah Y. Memona and Hassan K. Khalil. Output regulation of nonlinear systems using conditional servocompensators. *Automatica*, 46:1119–1128, July 2010.

Nicholas W Miller, William W Price, and Juan J Sanchez-Gasca. Dynamic modeling of ge 1.5 and 3.6 wind turbine-generators. *GE-Power Systems Energy Consulting*, 2003.

S Muller, M Deicke, and Rik W De Doncker. Doubly fed induction generator systems for wind turbines. *Industry Applications Magazine, IEEE*, 8(3):26–33, 2002.

Van Cuong Nguyen. *Robust Nonlinear Control - Application to Airlaunch*. PhD thesis, University of Evry - Val d'Essonne, France, 2013.

OFGEN. 9 august 2019 power outage report. Technical report, OFGEM, 2019.

K. R. Padiyar and N. Prabhu. Modelling, control design and analysis of vsc based hvdc transmission systems. In *2004 International Conference on Power System Technology, 2004 (PowerCon 2004)*, volume 1, pages 774–779 Vol.1, Nov 2004. doi: 10.1109/ICPST.2004.1460096.

Graham Pannell, David Atkinson, Ruth Kemsley, Lee Holdsworth, Phil Taylor, and Oscar Moja. Dfig control performance under fault conditions for offshore wind applications. In *Electricity Distribution, 2005. CIRED 2005. 18th International Conference and Exhibition on*, pages 1–5. IET, 2005.

R Pena, JC Clare, and GM Asher. Doubly fed induction generator using back-to-back pwm converters and its application to variable-speed wind-energy generation. *IEE Proceedings-Electric Power Applications*, 143(3): 231–241, 1996.

Sridhar Seshagiri and Hassan K. Khalil. Robust output feedback regulation of minimum-phase nonlinear systems using conditional integrators. *Automatica*, 41:43–54, January 2005.